Physica B 405 (2010) 2034–2038

Contents lists available at ScienceDirect

Physica B

journal homepage: www.elsevier.com/locate/physb

Nuclear spin-lattice relaxation in carbon nanostructures

A.M. Panich [a,*], N.A. Sergeev [b]

[a] Department of Physics, Ben-Gurion University of the Negev, P.O. Box 653, Beer Sheva 84105, Israel
[b] Institute of Physics, University of Szczecin, 70-451 Szczecin, Poland

ARTICLE INFO

Article history:
Received 27 October 2009
Received in revised form
26 December 2009
Accepted 15 January 2010

Keywords:
Carbon nanostructures
Nuclear spin-lattice relaxation

ABSTRACT

Interpretation of nuclear spin-lattice relaxation data in the carbon nanostructures is usually based on the analysis of fluctuations of dipole–dipole interactions of nuclear spins and anisotropic electron–nuclear interactions responsible for chemical shielding, which are caused by molecular dynamics. However, many nanocarbon systems such as fullerene and nanotube derivatives, nanodiamonds and carbon onions reveal noticeable amount of paramagnetic defects with unpaired electrons originating from dangling bonds. The interaction between nuclear and electron spins strongly influences the nuclear spin-lattice relaxation, but usually is not taken into account, thus the relaxation data are not correctly interpreted. Here we report on the temperature dependent NMR spectra and spin-lattice relaxation measurements of intercalated fullerenes $C_{60}(MF_6)_2$ (M=As and Sb), where nuclear relaxation is caused by both molecular rotation and interaction between nuclei and unpaired electron spins. We present a detailed theoretical analysis of the spin-lattice relaxation data taking into account both these contributions. Good agreement between the experimental data and calculations is obtained. The developed approach would be useful in interpreting the NMR relaxation data in different nanostructures and their intercalation compounds.

1. Introduction

Nuclear spin-lattice relaxation measurements are known to be an effective tool in studying carbon nanostructures, providing information on the nature of molecular dynamics and phase transitions [1]. Interpretation of the nuclear spin-lattice relaxation data in the aforementioned nanostructures is usually based on the analysis of fluctuations of dipole–dipole interactions in hydrocarbon and fluorocarbon groups and of anisotropic electron–nuclear interactions responsible for chemical shielding anisotropy. These fluctuations are caused by molecular mobility. However, many nanocarbon systems such as fullerene and nanotube derivatives and their intercalation compounds [2–5], nanodiamonds [6–10] and carbon onions [11–13] reveal noticeable amount of paramagnetic defects, which originate from dangling carbon bonds or structural defects with unpaired electrons. Such defects are usually created during the sample preparation process. The interaction between nuclear and electron spins is known to strongly influence the nuclear spin-lattice relaxation. Another contribution might come from the interaction of nuclear spins with adsorbed paramagnetic oxygen molecules. The aforementioned "paramagnetic" contribution is usually not taken into account, though without this the relaxation data cannot be correctly interpreted. Just such a case, when nuclear relaxation is caused by both molecular dynamics and interaction between nuclei and unpaired electron spins, is discussed in the present paper.

Here we report on the temperature dependent nuclear magnetic resonance (NMR) spectra and spin-lattice relaxation measurements of carbon nanostructured compounds $C_{60}(MF_6)_2$ (M=As, Sb), in which MF_6^- complexes are intercalated into the interstitial sites of the C_{60} lattice [14]. The composition of these intercalation compounds was found to be $C_{60}(MF_6)_x$ with $x \approx 1.9$ [14,15]. The study of the infrared (IF) spectrum hasidentified the octahedral structure of the AsF_6^- ion [15–17]. The frequency shift in the far IF and Raman spectra was attributed to a charge transfer from intercalate species to C_{60}, which was found to be 2 *holes* per C_{60} molecule [18]. This finding was supported by a reduction in the ^{13}C chemical shielding anisotropy of $C_{60}(MF_6)_2$ in comparison to solid C_{60} that was assigned to the charge transfer between C_{60} and intercalated species [3]. Electrical resistance of the compounds shows an exponential increase on cooling as is typical for semiconductor behavior [16]. The conduction is considered to be by holes. The ^{13}C NMR study of $C_{60}(MF_6)_2$ [3] showed that fullerene molecules are not mobile at temperatures up to 360 K, while room temperature ^{19}F spectra were found to be characteristic for rotating MF_6^- complexes [4]. Electron paramagnetic resonance (EPR) spectra of $C_{60}(AsF_6)_2$ and $C_{60}(SbF_6)_2$ compounds exhibit intense signal originating from unpaired electrons of dangling

* Corresponding author. Tel.: +972 8 6472458; fax: +972 8 6472903.
E-mail address: pan@bgu.ac.il (A.M. Panich).

0921-4526/$ - see front matter © 2010 Elsevier B.V. All rights reserved.
doi:10.1016/j.physb.2010.01.097

bonds [5]. This finding was supported by magnetic susceptibility measurements [5].

We note that although molecular dynamics of AsF_6 and SbF_6 complexes in graphite-intercalation compounds, clathrates, potassium hexafluoroarsenates and hexafluoroantimonates was studied by means of NMR [18–24], those studies were restricted by consideration of the motional average of dipole–dipole interactions and have never taken into account the interaction of nuclear spins with the spins of localized unpaired electrons. The latter is the main goal of our work, in which we report on the temperature dependent NMR spectra and spin-lattice relaxation measurements of intercalated fullerenes $C_{60}(MF_6)_2$ (M=As and Sb), where nuclear relaxation is caused by both molecular rotation and interaction between nuclei and unpaired electron spins, and present a detailed theoretical analysis of the spin-lattice relaxation and second moment data taking into account both these contributions. Such an approach will be useful in interpreting the NMR relaxation data in different nanostructures and their intercalation compounds.

2. Experimental details

Two powder samples $C_{60}(SbF_6)_2$ and $C_{60}(AsF_6)_2$, whose preparation is described elsewhere [3–5,14–17,25], were studied. The ^{19}F NMR measurements were carried out using a Tecmag pulse NMR spectrometer and Varian electromagnet in the temperature range from 67 to 365 K. Higher temperature would lead to the sample decomposition. The spectra at the resonance frequency 33.07 MHz (B_0=0.824 T) were recorded using Fourier transformation of the phase cycled solid echo. The lineshapes were intermediate between the Gaussian and Lorentzian functions. The second moments of the spectra, M_2, were calculated using a computer program by a standard procedure: $M_2=\frac{B_j-B_{j-1}}{A}\sum_{j=1}^{m}(B_j-B_0)^2y_j$ with $A=\sum_{j=1}^{m}(B_j-B_{j-1})y_j$. Spin-lattice relaxation times in the laboratory frame T_1 were measured using inversion recovery π-τ-$\pi/2$ sequence.

3. Calculations and analysis of experimental results

In this section we analyse the obtained experimental results assuming that the second moments of ^{19}F NMR spectra and the ^{19}F spin-lattice relaxation times in $C_{60}(SbF_6)_2$ and $C_{60}(AsF_6)_2$ samples are determined by both dipolar interactions between fluorine nuclei and interactions between fluorine nuclei and unpaired electron spins of paramagnetic defects. We will start with a calculation of the spin-lattice relaxation rates and second moments of the spectra and then will compare the results of the calculations with the experimental data.

We note that usually NMR data analysis requires taking into account also the contributions coming from the chemical shift anisotropies and difference in chemical shifts for inequivalent fluorine nuclei. In the case in question, consideration of such contributions would increase the number of fitting parameters and would make the analysis very complicated and not reliable enough. To avoid such a complication, we have carried out low-field measurements, in which the aforementioned contributions are negligible. Indeed, the ^{19}F chemical shielding anisotropy (CSA) of fluorine involved into Sb–F bond does not exceed 175 ppm in the rigid lattice [23,26]. Thus, the contribution of the CSA to the second moment $M_2=(4/45)(\sigma_{//}-\sigma_{\perp})^2$ [27] in the magnetic field of 0.824 T used in the experiment is found to be less than 3 kHz^2, which is much smaller than the experimental value caused by the dominating dipole–dipole interactions (see Section 3.2). Since arsenic is a light atom compared with antimony, the ^{19}F CSA contribution for the As–F bond is expected to be smaller than that for the Sb–F bond and thus is even more so negligible. Such an approach allows avoiding of a multi-parameter character of the problem under study and makes the analysis simpler and more reliable.

3.1. Temperature dependence of the spin-lattice relaxation rate

Nuclear spin-lattice relaxation rate $R_1\equiv T_1^{-1}$ is determined by the expression [28,29]

$$R_1=R_{1F}+R_{1F-X}. \tag{1}$$

Here $R_{1F}=T_{1F}^{-1}$ is the contribution to the spin-lattice relaxation rate caused by dipole–dipole coupling between spins of magnetic nuclei in rotating MF_6 groups, and $R_{1F-X}=T_{1F-X}^{-1}$ is the contribution caused by dipole–dipole interaction of fluorine nuclear spins and magnetic moments of paramagnetic defects. The first contribution is known to be described by the Bloembergen–Purcell–Pound (BPP) theory [28,29] and is given by the expression

$$R_{1F}\equiv T_{1F}^{-1}=\frac{2}{3}\frac{\Delta M_{2F}}{\omega_0}\left[\frac{x}{1+x^2}+\frac{4x}{1+4x^2}\right], \tag{2}$$

where $\omega_0=\gamma B_0$ is the Larmor frequency, $\tau_c=\tau_0\exp(E_a/RT)$ is the correlation time of the molecular rotation, $x=\omega_0\tau_c$, $\Delta M_{2F}=M_{2F}-\langle M_{2F}\rangle$ is the reduction of the second moment caused by the rotation of the molecular groups MF_6, M_{2F} the second moment of the rigid lattice, and $\langle M_{2F}\rangle$ the second moment of the NMR spectrum averaged by molecular motion [29]. The second contribution, coming from the dipole–dipole interaction of fluorine nuclear spins and unpaired electron spins of paramagnetic defects, is given by the expression [29,30]

$$R_{1F-X}\equiv T_{1F-X}^{-1}=\gamma_F^2\langle H_L^2\rangle\cdot\frac{\tau_{ce}}{1+(\omega_0\cdot\tau_{ce})^2}. \tag{3}$$

where $\langle H_L^2\rangle$ is determined as

$$\langle H_L^2\rangle=\frac{2}{5}\mu_p^2\frac{N_p}{N_F}\sum_i R_{ij}^{-6}. \tag{4}$$

Here $\mu_p^2=J(J+1)\gamma_j^2\hbar^2$is the squared magnetic moment of the paramagnetic defect, N_p the density of the paramagnetic defects (i.e., the number of paramagnetic defects in the volume unit), N_F the volume density of the fluorine atoms, τ_{ce} the correlation time that describes the reorientation of the electron spin caused by electron spin-lattice relaxation, and R_{ij} the distance from the jth paramagnetic center to the ith ^{19}F nucleus.

As it was shown by Panich et al. [4,5], the $C_{60}(SbF_6)_2$ and $C_{60}(AsF_6)_2$ compounds exhibit two structurally inequivalent MF_6 groups and two kinds of paramagnetic centers. Therefore, the experimental temperature dependences of the spin-lattice relaxation rate in these compounds were approximated by an expression

$$T_1^{-1}=\frac{2}{3}\Delta M_{2F}\cdot\left[\frac{\tau_c}{1+(\omega_0\tau_c)^2}+\frac{4\tau_c}{1+(2\omega_0\tau_c)^2}\right]+\gamma_F^2\langle H_L^2\rangle_1\frac{\tau_{ce1}}{1+(\omega_0\cdot\tau_{ce1})^2}+\gamma_F^2\langle H_L^2\rangle_2\frac{\tau_{ce2}}{1+(\omega_0\cdot\tau_{ce2})^2}. \tag{5}$$

Here τ_{cei} (i=1,2) are the correlation times, which are defined by the lifetimes of the electronic spin states and are determined from electron spin-lattice relaxation times T_{1e} [29]. As shown by Abragam [29], the correlation times τ_{cei} of electron spins of the paramagnetic centers and the correlation time τ_c caused by the rotations of the MF_6 groups usually follow the Arrhenius-type temperature dependence: $\tau_{cei}=\tau_{0e}\exp(E_{ei}/RT)$, ($i$=1, 2) and $\tau_c=\tau_0\exp(E_a/RT)$, respectively. Such dependence was used in our calculations. Under calculations, we supposed that the rotation

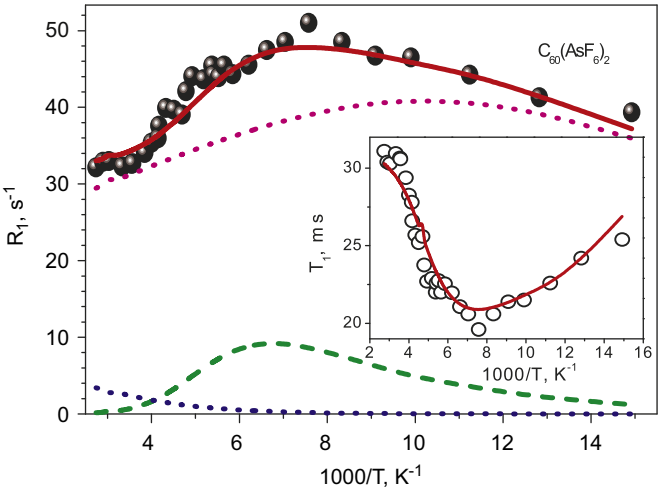

Fig. 1. Temperature dependence of the ^{19}F spin-lattice relaxation rate R_1 in $C_{60}(AsF_6)_2$ (circles). Red solid line is the calculated curve of Eq. (5) with the parameters given in Tables 1 and 2. The $R_{1F}(T)$ contribution to the relaxation rate is shown by dash green line. The contributions $R_{1F-X}(T)$ to the relaxation rate coming from two paramagnetic centers are shown by dotted blue and rose lines, respectively. Insert shows temperature dependence of the ^{19}F spin-lattice relaxation time T_1 in $C_{60}(AsF_6)_2$. For interpretation of the references to colour in this figure legend, the reader is referred to the web version of this article.

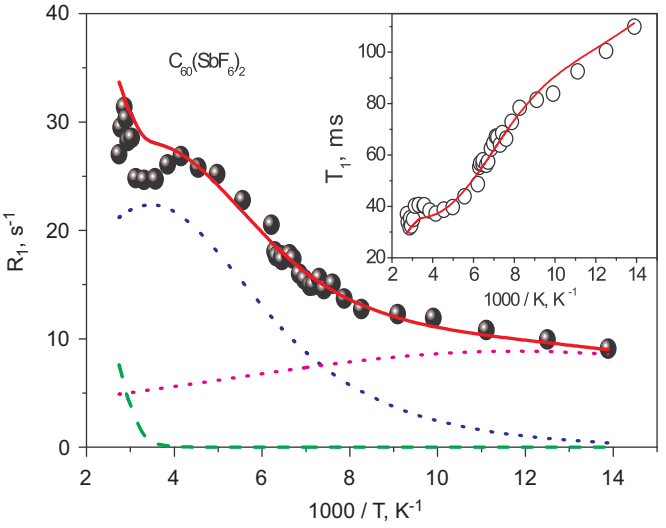

Fig. 2. Temperature dependence of the ^{19}F spin-lattice relaxation rate R_1 in $C_{60}(SbF_6)_2$ (circles). Red solid line is the calculated curve of Eq. (5) with the parameters given in Tables 1 and 2. The $R_{1F}(T)$ contribution to the relaxation rate is shown by dash green line. The contributions $R_{1F-X}(T)$ to the relaxation rate coming from two paramagnetic centers are shown by dotted blue and rose lines, respectively. Insert shows temperature dependence of the ^{19}F spin-lattice relaxation time T_1 in $C_{60}(SbF_6)_2$. For interpretation of the references to colour in this figure legend, the reader is referred to the web version of this article.

processes of the MF_6 groups are dynamically heterogeneous (i.e., are described by different activation energies E_a) and, accordingly, are characterized by a normal distribution of the activation energies

$$p(E_a) = \frac{1}{\sqrt{2\pi\sigma_E}} \exp\left\{\frac{E_a - \overline{E}_a}{2\sigma_E^2}\right\}. \quad (6)$$

Therefore, under calculations the first term in Eq. (5) was averaged over distribution function of Eq. (6). It is well known

Table 1
Calculated parameters that describe the contribution $R_{1F} \equiv T_{1F}^{-1}$ to the spin-lattice relaxation.

Compound	$\Delta M_{2F}=(M_{2F}-\langle M_{2F}\rangle)$ (kHz^2)	τ_0 (s)	$\overline{E}_a$ (kcal/mol)	σ_E (kcal/mol)
$C_{60}(AsF_6)_2$	130	10^{-13}	2.8	0.84
$C_{60}(SbF_6)_2$	52	10^{-13}	8	0.24

Table 2
Calculated parameters that describe the contribution $(R1_{F-X})_i$ $i=1, 2$ to the spin-lattice relaxation.

Compound	$\gamma_F^2\langle H_L^2\rangle_1$, $(rad \times kHz)^2$	$\gamma_F^2\langle H_L^2\rangle_2$, $(rad \times kHz)^2$	τ_{0e} (s)	E_{e1} (kcal/mol)	E_{e2} (kcal/mol)
$C_{60}(AsF_6)_2$	1700	17000	1.5×10^{-9}	1.3	0.225
$C_{60}(SbF_6)_2$	9300	3700	10^{-9}	0.9	0.265

that a normal distribution of the activation energies is equivalent to a log-normal distribution of the correlation times τ_c [31,32]. The experimental temperature dependences of the spin-lattice relaxation rates and the results of their approximation by function of Eq. (5) are presented in Figs. 1 and 2. The obtained adjusting parameters are given in Tables 1 and 2. One can find that satisfactory agreement between the experimental data and calculations is obtained. Fig. 1 shows that the temperature dependence of R_1 in $(AsF_6)_2C_{60}$ is typical for activation of molecular mobility on heating, thus the relaxation minimum at $T \sim 130$ K appears mainly due to fluctuations of dipole–dipole interactions of fluorine spins caused by the molecular rotation. The intercalated hexafluoride complex SbF_6^- is larger than AsF_6^- and experiences more hindrance in its reorientation in the interstitial cavity. Thus its mobility starts to appear at higher temperature in comparison to that of AsF_6^-. Therefore, the relaxation minimum in SbF_6^- caused by fluctuations of dipole–dipole interactions of fluorine spins would appear above 365 K, i.e., beyond the temperature range under study. The above conclusion is well supported by the temperature dependences of the second moments of the NMR spectra presented in the next subsection.

3.2. Temperature dependences of the second moments

The second moment of the NMR spectrum is given by the expression [29]

$$M_2 = M_{2F} + M_{2F-X}, \quad (7)$$

where M_{2F} is the contribution to M_2 coming from the dipole–dipole coupling of magnetic nuclei in rotating MF_6 groups and M_{2F-X} the contribution to M_2 arising from the dipole–dipole interaction between fluorine nuclear spins and magnetic moments of the paramagnetic defects. Rotation of the MF_6 groups yields narrowing of the NMR spectrum, and temperature dependence of M_{2F} (T) is given by the Gutowsky–Pake formula [28,29,33]:

$$M_{2F}(T) = \langle M_{2F}\rangle + (M_{2F} - \langle M_{2F}\rangle) \cdot \frac{2}{\pi} arctg(\delta\omega \cdot \tau_c), \quad (8)$$

where $\delta\omega \cong \sqrt{M_{2F}}$. The contribution to the second moment resulting from the interaction with the paramagnetic centers is also temperature dependent due to flips of the electron spins caused by electron spin-lattice relaxation [29,34]

$$M_{2F-X}(T) = \langle M_{2F-X}\rangle + \Delta M_{2F-X} \cdot \frac{2}{\pi} arctg(\delta\omega \cdot \tau_{ce}), \quad (9)$$

where τ_{ce} is the electron correlation time

$$\langle M_{2F-X}\rangle = \frac{3}{2}\left(\frac{\mu_p\omega_0}{3k_B(T-\theta)}\right)^2\langle H_L^2\rangle, \quad (10)$$

$$\Delta M_{2F-X} = \frac{1}{2}\gamma_F^2\langle H_L^2\rangle, \quad (11)$$

here $\langle H_L^2\rangle$ in Eqs. (10) and (11) is given by Eq. (4), k_B is the Boltzmann constant, and θ the Curie temperature.

Taking into account the existence of two paramagnetic centers in the sample, the experimental temperature dependences of the second moments of the NMR spectra of $C_{60}(SbF_6)_2$ и $C_{60}(AsF_6)_2$ were approximated by the expression

$$M_2(T) = A + B\frac{2}{\pi}arctg(\delta\omega\cdot\tau_c) + \frac{C_1}{(T-\theta)^2} + D_1\frac{2}{\pi}arctg(\delta\omega\cdot\tau_{ce1}) + \frac{C_2}{(T-\theta)^2} + D_2\frac{2}{\pi}arctg(\delta\omega\cdot\tau_{ce2}). \quad (12)$$

Here $A=\langle M_{2F}\rangle$; $B=M_{2F}-\langle M_{2F}\rangle$,

$$C_i = \frac{3}{2}\left(\frac{\mu_p\omega_0}{3k}\right)^2\langle H_L^2\rangle_i \quad (i=1,2), \quad (13)$$

$$D_i = \frac{1}{2}\gamma_F^2\langle H_L^2\rangle_i \quad (i=1,2). \quad (14)$$

Here Curie temperature was taken from the magnetic susceptibility data: $\theta=-8.7$ K for $C_{60}(AsF_6)_2$ and $\theta=-0.7$ K for $C_{60}(SbF_6)_2$ [5].

Broadened transition region in the experimental temperature dependences of the second moments of the NMR spectra indicates a distribution of the activation parameters of the rotating MF_6 groups. Therefore, in our calculations we assumed that the reorientation processes are not uniform and are described by a normal distribution of the activation energies given by Eq. (6). The experimental and calculated temperature dependences of the second moments of the ^{19}F NMR spectra are shown in Figs. 3 and 4. The obtained adjusting parameters are given in Tables 3 and 4. Good agreement between the experimental data and calculations is obtained. The observed variations of the second moment are caused by molecular dynamics discussed in the previous subsection. One can find that the main contribution to the second moment comes from the dipole–dipole coupling between fluorine spins, while the "paramagnetic" contribution starts to occur at low temperatures.

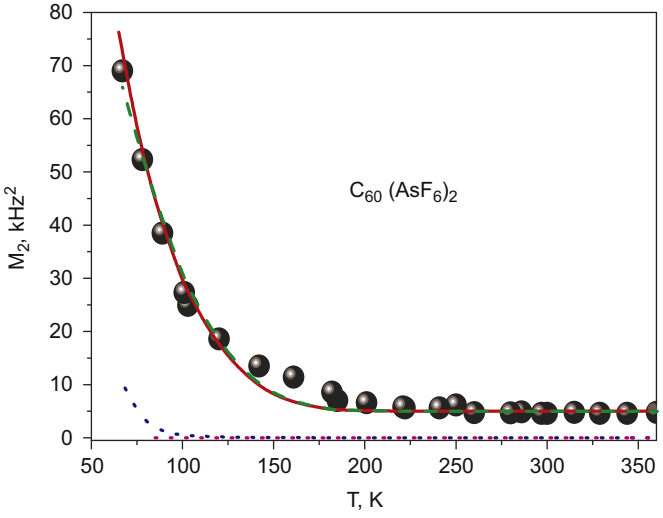

Fig. 3. Temperature dependence of the second moment of ^{19}F NMR spectrum in $C_{60}(AsF_6)_2$ (circles). Solid red line is the calculated curve of Eq. (12) with the parameters presented in Tables 3 and 4. The $M_{2F}(T)$ contribution to the second moment $M_2(T)$ is shown by dashed green line. The contributions $M_{2F-X}(T)$ to the second moment $M_2(T)$ coming from two paramagnetic centers are shown by solid blue and dashed rose lines. For interpretation of the references to colour in this figure legend, the reader is referred to the web version of this article.

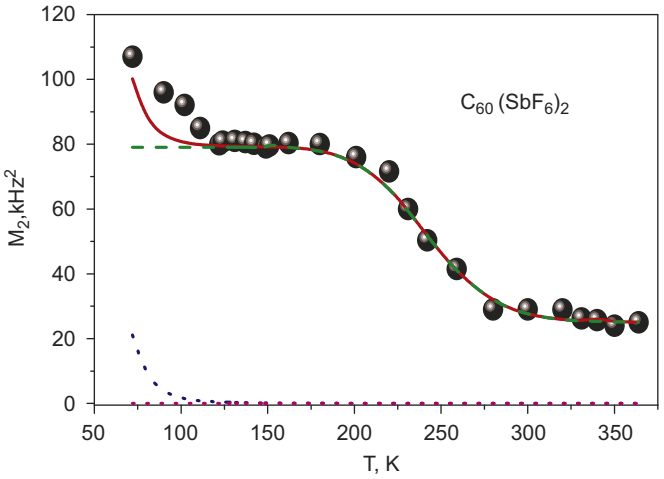

Fig. 4. Temperature dependence of the second moment of ^{19}F NMR spectrum in $C_{60}(SbF_6)_2$ (circles). Solid red line is the calculated curve of Eq. (12) with the parameters presented in Tables 3 and 4. The $M_{2F}(T)$ contribution to the second moment $M_2(T)$ is shown by dashed green line. The contributions $M_{2F-X}(T)$ to the second moment $M_2(T)$ coming from two paramagnetic centers are shown by solid blue and dashed rose lines. For interpretation of the references to colour in this figure legend, the reader is referred to the web version of this article.

Table 3
Parameters A, B, and $\gamma_F^2\langle H_L^2\rangle_i$ in Eq. (12).

Compound	A (kHz^2)	B (kHz^2)	$\gamma_F^2\langle H_L^2\rangle_1$ (kHz^2)	$\gamma_F^2\langle H_L^2\rangle_2$ (kHz^2)
$C_{60}(AsF_6)_2$	5	125	45	440
$C_{60}(SbF_6)_2$	25	54	210	90

Table 4
Parameters $\tau_{0e}, E_{e1}, E_{e2}, \tau_0, \overline{E_a}$ and σ_E in Eq. (12).

Compound	τ_{0e} (s)	E_{e1} (kcal/mol)	E_{e2} (kcal/mol)	τ_0 (s)	$\overline{E}_a$ (kcal/mol)	σ_E (kcal/mol)
$C_{60}(AsF_6)_2$	1.5×10^{-9}	1.3	0.225	10^{-13}	2.4	1.68
$C_{60}(SbF_6)_2$	10^{-9}	1.35	0.25	10^{-13}	9.5	0.95

4. Discussion

One can find from Figs. 1–4 that satisfactory agreement between the experimental data and calculations for the temperature dependences of both nuclear spin-lattice relaxation rates and second moments of the NMR spectra is obtained when the contribution resulting from the interaction of nuclear spins with the spins of the unpaired electrons is taken into account. This contribution is shown to be of significant importance for the relaxation rate. The obtained difference in the contributions to the nuclear spin-lattice relaxation coming from the two paramagnetic centers is caused by different amounts of these centers and by the difference in their activation energies and the electron spin-lattice relaxation times (see Tables 2 and 4).

From the data represented in Table 3 it follows that $M_{2F}(AsF_6)\cong 130$ and $M_{2F}(SbF_6)\cong 80$ kHz^2. These values of M_{2F}

Table 5
Parameters $\langle H_L^2 \rangle_i$ determined from M_2 and T_2 measurements.

Compound	$\langle H_L^2 \rangle_1$, G^2		$\langle H_L^2 \rangle_2$, G^2	
	from M_2	from T_1	from M_2	from T_1
$C_{60}(AsF_6)_2$	2.8	2.68	27.4	26.8
$C_{60}(SbF_6)_2$	13.1	14.7	5.6	5.8

are similar to the calculated contributions into $M_{2F}=M_{2F-F}+M_{2F-M}$ coming from the dipole–dipole coupling among the fluorine spins M_{2F-F} and from the interactions of the fluorine spins and spins of nuclei M in the MF_6 groups, M_{2F-M}: $M_{2F}(AsF_6)=M_{2F-F}+M_{2F-As}=114.3+16=13.0\,\mathrm{kHz}^2$ $M_{2F}(SbF_6)=M_{2F-F}+M_{2F-Sb}=67+34=101\,\mathrm{kHz}^2$. At that, the contribution to the second moment resulting from the Curie–Weiss-like term $C_1/(T-\theta)^2$ (Eq. 12) was found to be negligible in comparison with that of the $(2/\pi)arctg(\delta\omega\cdot\tau_c)$ term. We note that the calculated activation energy of the first paramagnetic center is approximately five times larger that that of the second center. Therefore, the contribution to M_2 coming from the dipolar coupling of the ^{19}F nuclei with the unpaired electrons of the second center is nearly averaged out and only contribution from the first center remains in the temperature range under study, as it is seen from Figs. 3 and 4. Let us now discuss the values of $\langle H_L^2 \rangle_i$ using the data presented in Tables 2 and 4, and the values of $\langle H_L^2 \rangle_i$ determined from the M_1 and T_1 measurements that are given in Table 5. Noginova et al. [35] proposed the following formula for $\langle H_L^2 \rangle$

$$\langle H_L^2 \rangle = 0.4\frac{16\pi^3}{9}N_p^2 J(J+1)\gamma_p^2\hbar^2 = 14N_p^2\mu_p^2 \tag{15}$$

Using Eq. (15), one can obtain the expression for the concentration of the paramagnetic centers

$$N_p = \frac{0.27}{\mu_p}\sqrt{\langle H_L^2 \rangle}. \tag{16}$$

Assuming that $\mu_p=\mu_B$ (here μ_B is the Bohr magneton) and using the data presented in Table 5, we calculated the concentrations of the paramagnetic defects as $N_{p1}\cong 5\times10^{19}\,\mathrm{cm}^{-3}$, $N_{p2}\cong 1.6\times10^{20}\,\mathrm{cm}^{-3}$, $N_p=N_{p1}+N_{p2}=2.1\times10^{20}\,\mathrm{cm}^{-3}$ in $C_{60}(AsF_6)_2$ and $N_{p1}\cong 1.1\times10^{20}\,\mathrm{cm}^{-3}$, $N_{p2}\cong 7\times10^{19}\,\mathrm{cm}^{-3}$, $N_p=N_{p1}+N_{p2}=1.8\times10^{20}\,\mathrm{cm}^{-3}$ in $C_{60}(SbF_6)_2$.

One can find that $C_{60}(AsF_6)_2$ exhibits somewhat larger density of paramagnetic defects than $C_{60}(SbF_6)_2$, in agreement with the magnetic susceptibility and EPR data [5].

5. Conclusion

We reported on the temperature dependent NMR spectra and spin-lattice relaxation measurements of the carbon nanostructured compounds $C_{60}(MF_6)_2$ (M=As, Sb), in which MF_6 complexes are intercalated into the C_{60} lattice. Nuclear relaxation in these compounds is caused by both molecular dynamics and interaction between nuclear spins and unpaired electron spins. We made a detailed theoretical analysis of the spin-lattice relaxation data taking into account both aforementioned contributions. Satisfactory agreement between the experimental data and calculations was obtained. We believe that the approach developed in this paper would be useful in interpreting the NMR relaxation data in different nanostructures and their intercalation compounds.

Acknowledgements

One of the authors (A.M.P.) thanks W.R. Datars for supplying us with the samples of $C_{60}(AsF_6)_2$ and $C_{60}(SbF_6)_2$ and A.I. Shames for helpful discussion. on the EPR data. The work in Israel was supported by two Seed Money Grants of the Ben-Gurion University of the Negev.

References

[1] R. Tycko, G. Dabbagh, R.M. Fleming, R.C. Haddon, A.V. Makhija, S.M. Zahurak, Phys. Rev. Lett. 67 (1991) 1886.
[2] A.M. Panich, A.I. Shames, H. Selig, J. Phys. Chem. Solids 63 (2002) 483.
[3] A.M. Panich, P.K. Ummat, W.R. Datars, Solid State Commun. 121 (2002) 367.
[4] A.M. Panich, H.M. Vieth, P.K. Ummat, W.R. Datars, Physica B 327 (2003) 102.
[5] A.M. Panich, I. Felner, A.I. Shames, S. Goren, P.K. Ummat, W.R. Datars, Solid State Commun. 129 (2004) 81.
[6] A.I. Shames, A.M. Panich, W. Kempiński, A.E. Alexenskii, M.V. Baidakova, A.T. Dideikin, V. Yu. Osipov, V.I. Siklitski, E. Osawa, M. Ozawa, A. Ya. Vul', J. Phys. Chem. Solids 63 (2002) 1993.
[7] A.M. Panich, A.I. Shames, H.M. Vieth, E. Ōsawa, M. Takahashi, A. Ya. Vul', Eur. Phys. J. B 52 (2006) 397.
[8] A.I. Shames, A.M. Panich, S. Porro, M. Rovere, S. Musso, A. Tagliaferro, M.V. Baidakova, V. Yu Osipov, A. Ya Vul', T. Enoki, M. Takahashi, E. Osawa, O.A. Williams, P. Bruno, D.M. Gruen, Diamond Relat. Mater. 16 (2007) 1806.
[9] A.M. Panich, Diamond Relat. Mater. 16 (2007) 2044.
[10] G. Cunningham, A.M. Panich, A.I. Shames, I. Petrov, O. Shenderova, Diamond Relat. Mater. 17 (2008) 650.
[11] A.I. Shames, A.M. Panich, E. Mogilko, J. Grinblat, E.W. Prilutskiy, E.A. Katz, Diamond Relat. Mater. 16 (2007) 2039.
[12] A.I. Shames, E.A. Katz, A.M. Panich, D. Mogilyansky, E. Mogilko, J. Grinblat, V.P. Belousov, I.M. Belousova, A.N. Ponomarev, Diamonds Relat. Mater. 18 (2009) 505.
[13] E.A. Katz, A.M. Panich, D. Mogilyansky, E. Mogilko, J. Grinblat, V.P. Belousov, I.M. Belousova, A.N. Ponomarev, A.I. Shames, Cond-mat e-print archive, April 20, 2009, ⟨http://arxiv.org/abs/0904.2647⟩.
[14] W.R. Datars, T.R. Chien, R.K. Nkum, P.K. Ummat, Phys. Rev. B 50 (1994) 4937.
[15] W.R. Datars, P.K. Ummat, Solid State Commun. 94 (1995) 649.
[16] W.R. Datars, J.D. Palidwar, P.K. Ummat, J. Phys. Chem. Solids 57 (1996) 977.
[17] R. Francis, P.K. Ummat, W.R. Datars, J. Phys. Condens. Matter 9 (1997) 7223.
[18] E.R. Andrew, L.F. Farnell, T.D. Gledhill, Phys. Rev. Lett. 19 (1967) 6.
[19] H.A. Resing, F.L. Vogel, T.C. Wu, Mater. Sci. Eng. 41 (1979) 113.
[20] G.R. Miller, H.A. Resing, M.J. Moran, L. Banks, F.L. Vogel, A. Fron, D. Billaud, Synth. Met. 8 (1983) 77.
[21] M.J. Moran, G.R. Miller, R.A. Demarko, H.A. Resing, J. Phys. Chem. 88 (1984) 1580.
[22] G.C. Chingas, J. Milliken, H.A. Resing, T. Tsang, Synth. Met. 12 (1985) 131.
[23] Yu.N. Moskvich, B.I. Cherkasov, A.M. Polyakov, A.A. Suknovskii, R.L. Davidovich, Phys. Status Solidi B 156 (1989) 615.
[24] D.W. Davidson, J.A. Ripmeester, NMR NQR and dielectric properties of clathrates, in: J.L. Atwood, J.E.D. Davies, D.D. MacNicol (Eds.), Inclusion Compounds, Vol. 3, Academic Press, New York, 1984.
[25] J.C.L. Chow, P.K. Ummat, W.R. Datars, J. Phys. Condens. Matter 12 (2000) 8551.
[26] A.M. Panich, Synth. Met. 100 (1999) 169.
[27] N. Bloembergen, T.J. Rowland, Phys. Rev. 97 (1955) 1679.
[28] N. Bloembergen, E.M. Purcell, R.V. Pound, Phys. Rev. 73 (1948) 679.
[29] A. Abragam, The Principles of Nuclear Magnetism, Clarendon, Oxford, 1961.
[30] T.T. Phua, B.J. Beadry, D.T. Peterson, D.R. Torgeson, R.G. Barnes, M. Belhoul, G.A. Styles, E.F.W. Seymour, Phys. Rev. B 28 (1983) 6227.
[31] H.A. Resing, J. Chem. Phys. 43 (1965) 669.
[32] J.A. Ripmeester, Ch.I. Ratcliffe, I.G. Cameron, J. Phys. Chem. B 108 (2004) 929.
[33] H.S. Gutowski, G.E. Pake, J. Chem. Phys. 18 (1950) 162.
[34] A.L. Pigg, S.M. Day, Phys. Rev. B 11 (1975) 3219.
[35] N. Noginova, E. Arthur, T. Weaver, G.B. Loutts, V.A. Atsarkin, D.G. Gotovsev, Phys. Rev. B 69 (2004) 024406.